Article

Pressure dependent thermoreflectance spectroscopy induced by interband transitions in metallic nano-film

Zhongyin Zhang,
Zheng Chang,
Xuanhui Fan, ...,
Xiaoliang Zhang,
Jie Zhu, Dawei
Tang

zhujie@dlut.edu.cn (J.Z.)
dwtang@dlut.edu.cn (D.T.)

Highlights
Thermoreflectance (dR/dT) of Al films was measured under a pressure range of 0–25 GPa

A semi-quantum model well describes the pressure effect on optical properties

Pressure enlarges interband transition energy which makes dR/dT pressure-dependent

The resonant interband transitions let dR/dT change to negative at ~6 GPa

iScience

Article

Pressure dependent thermoreflectance spectroscopy induced by interband transitions in metallic nano-film

Zhongyin Zhang,[1] Zheng Chang,[1] Xuanhui Fan,[1] Jing Zhou,[1] Xinwei Wang,[2] Gen Li,[1] Xiaoliang Zhang,[1] Jie Zhu,[1,3,*] and Dawei Tang[1,*]

SUMMARY

Utilizing high-pressure to modulate optical properties, such as thermoreflectance (dR/dT), over a wide range has received much attention. Nevertheless, how the pressure exerts on the complex dielectric constant and finally on dR/dT remains elusive. Here, we perform a thoroughly experimental and theoretical investigation on dR/dT of Al nano-film from 0 to 25 GPa. The dR/dT values exhibit a sine-like pressure-dependence, with the zero-crossing appearing at around 6 GPa. These special phenomena are well explained from electron transition viewpoints. The *first-principles* calculations show that the energy difference of parallel bands is enlarged from 1.45 to 2 eV, thereby increasing the threshold for electron transitions. The lifted threshold changes the optical absorption rates of Al and the density of states of the electrons involving interband transitions; finally, the resulting dR/dT exhibits such a pressure-dependent behavior. Our findings provide a deep insight on pressure-induced electronic transitions and photon-electron interactions in metals.

INTRODUCTION

Physical properties of materials at high pressure are of great importance in geophysics, astrophysics, and high temperature superconductors. The investigation of physical properties at high pressure is capable of providing fundamental insights into properties of condensed matter that is not otherwise clear from ambient pressure experiments. Recently, utilizing high pressure to realize the modulation of physical properties has also received a great deal of attention. Numerous studies have confirmed that pressure on the gigapascal scale enabled us to alter optical (Jaffe et al., 2016; Xiao et al., 2017), mechanical (Liu et al., 2020; Zhao et al., 2017), and thermal properties (Hohensee et al., 2015a; Hsieh et al., 2011) of materials over a wide range. Among them, high-pressure thermoreflectance (dR/dT) spectroscopy can be used for yielding important information of materials, such as detailed electronic band structure, optical absorption at critical points in the Brillouin zone, photon-electron interactions, and optical transitions involving the Fermi level (Colavita et al., 1983a, 1983b; Hanus et al., 1967; Smith and Norris, 2001). The dR/dT of metals at high pressure also contains the information of both the normal ground-state electronic properties and the effect of many scattering electrons (Tups and Syassen, 1984).

Thermoreflectance spectroscopy of metals have been studied for decades (Eesley, 1983; Hopkins, 2009, 2010a; Rosei, 1974; Rosei et al., 1974; Tups and Syassen, 1984). Rosei and his co-workers (Rosei and Lynch, 1972) measured the dR/dT of Al, Au, and Cu at 120 and 370 K and ambient pressure in photon energy range of 0.5–5 eV and the data yielded the dR/dT spectrum of the imaginary part of the dielectric constant directly, without the Kramers-Kronig analysis. In particular, they found that the imaginary part of the dielectric constant of Al was able to be discussed simply using closed-form expressions for optical conductivity, and intraband transitions dominated the dR/dT at the infrared region. Subsequently, Tups and Syassen (Tups and Syassen, 1984) first made a significant stride towards the effect of pressure on the optical absorption in Al. With the pressure increasing, the spectrum of reflectivity (R) had a slightly increasing discrepancy in the shape of the absorption edges, resulting in that the R changed slightly with pressure at fixed photon energy. Dandrea and Ashcroft (Dandrea and Ashcroft, 1985) further correlated electron scattering with the optical absorption features of Al at high pressure. They found that the experimental data in earlier work (Tups and Syassen, 1984) were best accounted for when scattering effects were included within a

[1]School of Energy and Power Engineering, Key Laboratory of Ocean Energy Utilization and Energy Conservation of Ministry of Education, Dalian University of Technology, Dalian 116024, Liaoning, P. R. China

[2]College of New Energy, China University of Petroleum (East China), Qingdao 266580, Shandong, P. R. China

[3]Lead contact

*Correspondence: zhujie@dlut.edu.cn (J.Z.), dwtang@dlut.edu.cn (D.T.)

https://doi.org/10.1016/j.isci.2021.102990

number-conserving approximation, and when an *ab initio* electron-electron scattering rate was also included. In fact, it should be noted that very little work has been carried out on pressure effect on *dR/dT*.

Moreover, when investigating the pressure effect on thermal transport properties, the experiment technique was limited to optical methods, such as time domain thermoreflectance (TDTR), which is a multi-functional and non-contact pump-probe method and requires a metallic transducer film. The fundamental principles of TDTR directly relate to *dR/dT* of metallic films as thermometers (Cahill, 2004), which can be considered as a constant when the temperature change is small. Therefore, the value of *dR/dT* of metallic films is critical for the optimization of TDTR signals. In addition, the combination of TDTR and a diamond anvil cells (DAC) (Jayaraman, 1986) enables us to investigate both optical (Chen et al., 2016; Zheng et al., 2018) and thermal (Hohensee et al., 2015a; Hsieh et al., 2011) properties at high pressure systematically, in which Al nano-film is the most widely used transducer because of its high *dR/dT* and high stability. Hence, the pressure dependence of *dR/dT* of Al is also of great importance in the studies of high pressure thermophysics.

Literature studies on the microscale regime of thermoreflectance spectroscopy in ambient-pressure TDTR measurements had indicated that the change of thermal reflectance signals from a metal film could be caused by the change of the plasma frequency, carrier scattering rates, and the number density of electronic population around the Fermi surface (Hopkins, 2010b). Wang et al. (Wang et al., 2010) and Wilson et al. (Wilson et al., 2012) reported the values of *R* and *dR/dT* for different metals and oxides at wavelength range 0.4–1.6 μm and those data assisted in the design and interpretation of optical pump-probe studies of thermal properties. For the experiments under high pressure, Hsieh and Cahill (Hsieh and Cahill, 2011) measured the *dR/dT* of Ta, Au(Pd) ($\approx$ 5 at. % Pd), and Al by combining TDTR and a silicon carbide anvil cell. They found that Ta had a large and pressure-independent *dR/dT* within 10 GPa (Wang et al., 2010), whereas Au(Pd) had a very high *R* at the wavelength of 785 nm but a too weak *dR/dT* (Hohensee et al., 2015b). The *dR/dT* of Al was very sensitive to pressure and decreased to near zero when the pressure increased to around 6 GPa.

Therefore, different metal materials showed various pressure-dependent *dR/dT* spectroscopies, whereas the physical mechanism of this pressure-effect remains elusive owing to the challenges in both accurate measurements and sophisticated modeling. Herein, we presented both experimental and theoretical studies on *R* and *dR/dT* of Al at high pressure. Firstly, four samples, i.e., Al/GaAs, Al/SiO$_2$/Si, Al/ZnO, and Al/SrTiO$_3$ were prepared (see STAR Methods), and their *R* and *dR/dT* were measured by TDTR integrated with a DAC in the pressure range of 0–25 GPa; the schematic diagram is shown in Figure 1. The pressure gradient as a function of pressure is shown in Figure S1. Then, we proposed a new theoretical method, in which classical and quantum-mechanical dielectric functions were taken into consideration, to quantify pressure-dependent *R* and *dR/dT*, with the electronic band structure using *first-principles* calculations. Finally, by comparing the experimental and theoretical results, the behaviors of *R* and *dR/dT* of Al at high pressure were well explained by interband transitions and energy-band engineering.

RESULTS AND DISCUSSION
Measurements on reflectivity as a function of pressure

Figure 2A shows the measured V_{dc} signals normalized by probe beam energy (see STAR Methods) of Al/GaAs, Al/SiO$_2$/Si, Al/ZnO, and Al/SrTiO$_3$ as functions of pressure. The V_{dc} signals of the Al/GaAs and Al/SiO$_2$/Si, which are measured in the air, are 77 mV. When the samples are loaded into the DAC, the V_{dc} signals reduced to $\approx$ 55% for the reflection of two interfaces (diamond/air and diamond/silicone-oil), and the schematic diagram is inserted in Figure 2A. For the normal incidence of the probe beam, the *R* of each interface is capable of being expressed as $R=(n_1-n_2)^2/(n_1+n_2)^2$, in which the refractive index of air, diamond, and silicone-oil were 1, 2.47, and 1.4, respectively. With the expression of the *R* used, we calculate the reflectivity of the diamond/silicone-oil interface $R_1 = 0.075$ and the diamond/air interface $R_2 = 0.18$. The probe beam normally passes through each interface twice, so we estimate the reduction of the V_{dc} signals by a factor of $(1-R_1)^2 \times (1-R_2)^2 = 0.55$. Therefore, the calculated V_{dc} signals of Al/GaAs and Al/SiO$_2$/Si in the DAC and at ambient pressure are 42.5 mV, which are well consistent with the experimental values.

In addition, we obtain the pressure dependence of the *R* using Equation (1) (STAR Methods), as shown in Figure 2B. There are some factors that contributed to the error of the *R* at high pressure. The uncertainty of
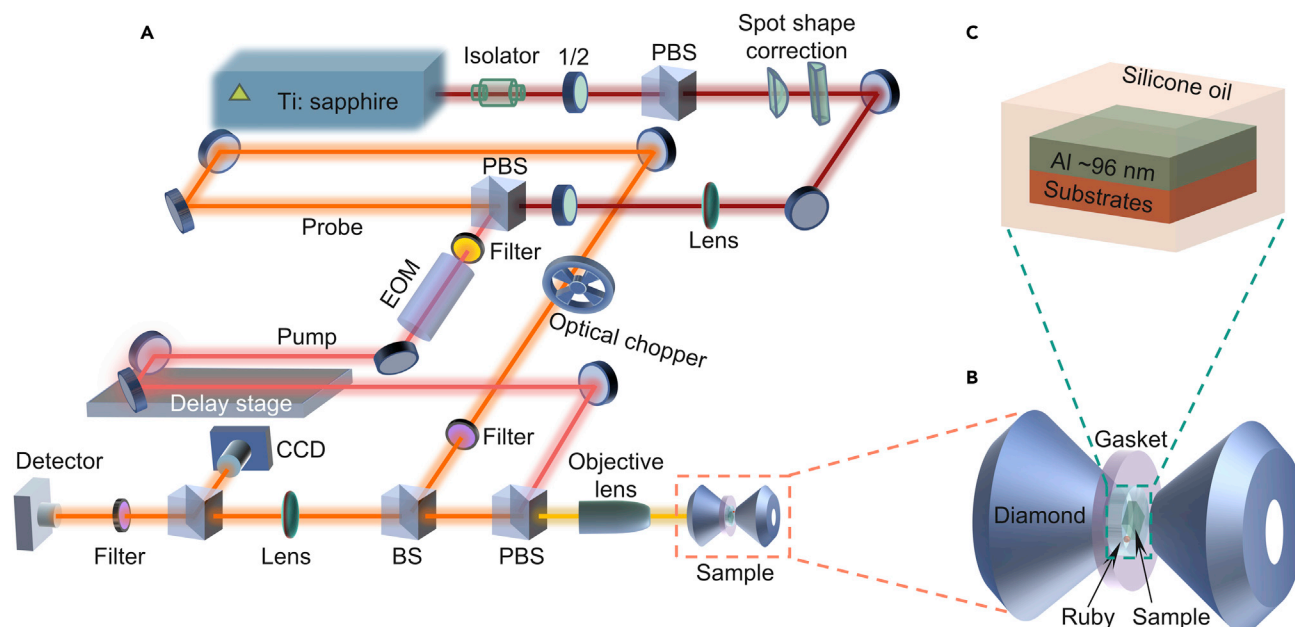
Figure 1. Schematic diagram of experimental setup for high-presure TDTR measurements

(A) Schematic of the TDTR system setup. The abbreviation of PBS, BS, and EOM stand for polarizing beam splitter, beam splitter, and electro-optic-modulator respectively.

(B) Configuration of the diamond anvil cell (DAC) with a sample chamber, rubies, and samples.

(C) The schematic of samples for the dR/dT and R measurements.

$V_{dc,p}$, which is generated by photodiode, is about 0.5%, the error of R_0 is within 5%, and the error of the estimated $V_{dc,0}$ is about 5%. Therefore, the total error of the R can be estimated as $E_R = \sqrt{E_{V_{dc,0}}^2 + E_{R_0}^2 + E_{V_{dc,p}}^2}$, which is approximatively 7%. The experimental results show that the R of Al/GaAs, Al/ZnO, and Al/SrTiO$_3$ is sensitive to pressure when pressure is above 10 GPa, and substrates have large effects on R at high pressure regions. This observation suggests that the R of Al nano-films can be affected by interfaces shear strains of Al/substrates, which can split degenerate energy bands and cause shifting and warping, and then affect the Fermi level. Moreover, the R is a surface phenomenon, so surface conditions may have a large effect on it. At such extreme environment, the Al film will undergo different plastic defor-mation, especially at high pressure conditions, to accommodate the substrates. Thus, different surface con-ditions such as roughness make differences in behavior in R. Those perspectives are supported by pressure dependence of the R of Al/diamond drawn from previous work (Hohensee et al., 2015b; Tups and Syassen, 1984), which are labeled in Figure 2B. In their experiments, the Al film was deposited on diamond anvil plates, whereas the stiffness of diamond is high enough so that the deformation is almost negligible. Hence the shear strains of Al/diamond interface are small, which somewhat protects the Al film and makes the R insensitive to pressure.

Measurements on thermoreflectance as a function of pressure

In Figure 3A, we plot the V_m signals normalized by pump beam energy versus pressure for the Al/GaAs, Al/SiO$_2$/Si, Al/ZnO, and Al/SrTiO$_3$. To inhibit the effect of pressure-induced inhomogeneity of the samples, we measure the V_m signals (see STAR Methods) at three to four locations under each pressure and select the average signals as the measurement results. As seen in Figure 3A, with the pressure increasing, the normalized V_m signals of these four samples decrease, and then down to negative. We also see the V_m sig-nals of Al films on these four substrates exhibit almost the same pressure-dependent behaviors. As ex-pected, the dR/dT of the Al/GaAs, Al/SiO$_2$/Si, Al/ZnO, and Al/SrTiO$_3$ (Figure 3B), which are figured out by Equation (2) (see STAR Methods), exhibits a parallel behavior with the normalized V_m signals. This obser-vation givea a direct experimental evidence that pressure is capable of reducing the dR/dT of Al nano-films at a laser wavelength of 785 nm, which dramatically alters the R temperature coefficients of electrons and phonons from positive to negative at around 6 GPa. To estimate the error of the dR/dT, it is essential for us to take the error propagation of the V_m, V_{dc}, R, and ΔT into consideration. With the variation of thermal
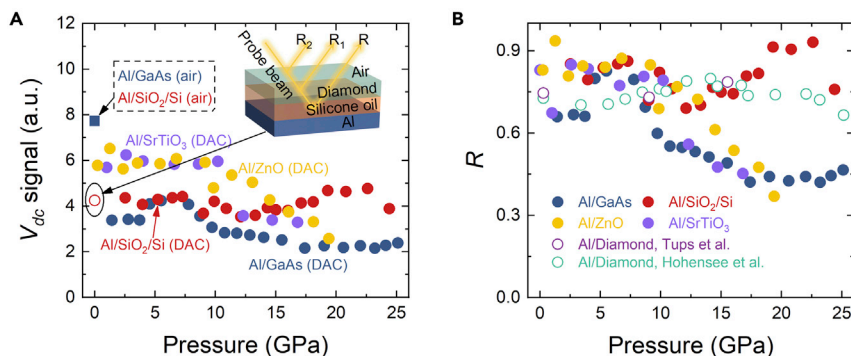
Figure 2. Normalized V_{dc} signals and R of Al as functions of pressure

(A) The V_{dc} signals normalized by probe beam energy of Al/GaAs, Al/SiO$_2$/Si, Al/ZnO, and Al/SrTiO$_3$ as a function of pressure. As shown in the schematic of multilayer reflection, after the samples are loaded into the DAC, the normalized V_{dc} signals measured in the air (filled squares) reduce to $\approx 55\%$ (hollow circles) due to the reflection of two interfaces. R, R$_1$ and R$_2$ denote the reflectivity of silicone-oil/Al, diamond/silicone-oil, and air/diamond interfaces, respectively. Filled circles denote the normalized V_{dc} signals at high pressure.

(B) Pressure dependence of the R of Al nano-films. The total error of the R is about 7%. The experimental results show that the R of Al/GaAs, Al/ZnO, and Al/SrTiO$_3$ is sensitive to pressure when pressure is above 10 GPa, and substrates have large effects on R at high pressure regions. As a comparison, we also draw the pressure dependence of Al/diamond (hollow circles) from literature.

parameters at high pressure, the error of ΔT is less than 7%, and the error of quality factor Q is typical 5%. Therefore, the total error was performed as $E_{dR/dT} = \sqrt{E_{V_m}^2 + E_{V_{dc}}^2 + E_Q^2 + E_R^2 + E_{\Delta T}^2}$, which is $\approx 14\%$.

As seen in Figure 3B, the dR/dT of the four samples at ambient pressure or low pressure are in the range of 1.6×10^{-4} K^{-1}-2.1×10^{-4} K^{-1}, which are consistent with literature (Favaloro et al., 2015; Wang et al., 2010; Wilson et al., 2012). Furthermore, we plot the dR/dT of the Al/mica and Al/diamond drawn from earlier work (Hohensee et al., 2015b; Hsieh and Cahill, 2011) in Figure 3B. The measured dR/dT of the four samples are consistent and in good agreement with literature values. Remarkably, we notice that the dR/dT of Al nano-films under different pressure spanned one to two orders of magnitude; however, R only changes slightly. In fact, it should be noted that very little available work has been carried out on explaining the behavior of the R and dR/dT of Al nano-films under high-pressure fundamentally. Therefore, to gain more insights, we also conducted the theoretical derivations (see STAR Methods) and *first-principle* calculations (see STAR Methods) to investigate the pressure-dependence of the R and dR/dT of Al quantitatively.

Theoretical calculations on reflectivity and thermoreflectance as functions of pressure

According to the theoretical derivations of the R and dR/dT, we find that only the energy difference ΔE_{ul} of the two bands involving interband transitions is a function of pressure and dominates the change in dR/dT of Al. Therefore, to obtain the relationship of ΔE_{ul} and pressure, we perform the *first-principles* calculations on the electronic band structure from ambient pressure to 25 GPa. In the calculations, we applied hydrostatic pressure conditions to obtain the band structure, and the lattice constants reduced isotropically. Figures 4A–4E show the band structure between **K** and **X** at several selected pressure, and the transition regions are marked by solid arrows. Almost all of interband transitions occur on the approximately parallel bands that are symmetric about the Γ point in the Brillouin zone and one is between **K** and **X**. The approximately parallel bands, one above the Fermi level E_f and the other below, enable the interband transitions from a large number of occupied states; however, below the E_f, all occur at the energy of ΔE_{ul}. Therefore, the density of states at the ΔE_{ul} are very high, resulting in a particularly strong absorption at this photon energy. In Figure 4F, we plot the calculated ΔE_{ul} as a function of pressure. We see that ΔE_{ul} increased monotonously with increasing pressure, and we fitted ΔE_{ul} with pressure by a 3rd polynomial fitting for guiding the eyes (labeled in Figure 4F). The band structures calculations suggest that enhanced optical absorption and interband transition rates at different ΔE_{ul} qualitatively demonstrate the evolution of R and dR/dT as functions of pressure.

To explain the relationship between R as well as dR/dT and pressure quantitatively, we, therefore, take both intraband and interband transitions into consideration when we perform the theoretical calculations. On
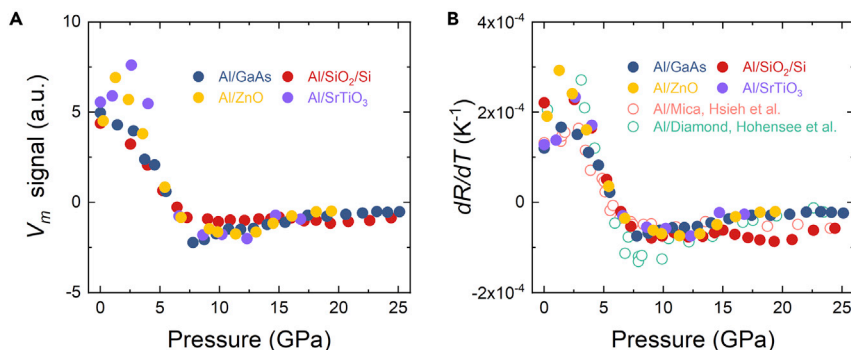
Figure 3. Normalized V_m signals and dR/dT of Al as functions of pressure

(A) The V_m signals normalized by pump beam energy versus pressure. With the pressure increasing, the normalized V_m signals and dR/dT of the Al/GaAs, Al/SiO$_2$/Si, Al/ZnO, and Al/SrTiO$_3$ decrease, and then down to negative. We also see the V_m signals of Al films on these four substrates exhibit almost the same pressure-dependent behaviors. The total error of the dR/dT is $\approx$ 14%.

(B) dR/dT of Al versus pressure. Filled circles denote the experimental results of the Al/GaAs (navy), Al/SiO$_2$/Si (dull red), Al/ZnO (yellow), and Al/SrTiO$_3$ (purple). Hollow circles represent the dR/dT of the Al/mica (pink) and Al/diamond (light green) drawn from literature.

the basis of the Equations 3–13 (see STAR Methods), we calculate the optical properties of Al as functions of photon energy and pressure, as shown in Figure 5. In Figures 5A, 5C, 5E, and 5G, we plot the ϵ, $\Delta\epsilon$, R, and dR/dT as functions of photon energy at ambient pressure, respectively. In this calculation, the ΔE_{ul} of ambient pressure is from the *first-principle* calculations and other input parameters are from literature (Rakić et al., 1998). Obviously, our calculated results, i.e., ϵ_1, ϵ_2, $\Delta\epsilon_1$, $\Delta\epsilon_2$, R, and dR/dT as functions of pressure, match well with reported value in previous work (Barron et al., 2007; Rakić et al., 1998; Wang et al., 2010; Wilson et al., 2012), indicating that our theoretical model is valid and robust.

As seen in Figures 5B, 5D, 5F, and 5H, we plot the ϵ, $\Delta\epsilon$, R, and dR/dT as functions of pressure, respectively. In Figure 5B, both ϵ_1 and ϵ_2 exhibit a relatively weak pressure dependence overall, implying that ΔE_{ul} slightly affects the dielectric constant as well as the R, which is calculated and shown in Figure 5F (blue line). Likewise, strong interband transitions make the real and imaginary parts of the $\Delta\epsilon$ to exhibit a large vibration at around 6 GPa, as shown in Figure 5D. Besides, in Figures 5F and 5H, we compare the experimental and theoretical results of R and dR/dT and find that the calculated results are in good agreement with the experimental results, especially at critical point regions (labeled in Figure 4F), where the strongest optical absorption and interband transitions occur. Our experimental and theoretical results indicate that, (1) pressure alters the optical absorption rates at photon energy of the probe beam and then makes R to exhibit a pressure dependent behavior. (2) The calculated results of pressure dependent R are consistent with the experimental results in low pressure regions, whereas the shear strains caused by Al/substrate have large effects on R at higher pressure conditions. In addition, the calculation results show that there should be a strong absorption at around 6 GPa, thus R of this pressure is supposed to be lower than that of other pressures; however, the experimental results do not capture this phenomenon. We attribute this difference to uneven surface conditions at high pressure conditions. (3) ΔE_{ul} is the energy threshold of interband transition and is near photon energy of the probe beam (1.58 eV) at around 6 GPa, resulting in that dR/dT of almost down to zero at this pressure. (4) Pressure can enlarge ΔE_{ul} of the parallel bands between **K** and **X** points in the Brillouin zone, and then change the density of states of electrons that involve interband transitions near the E_f; leading to that, dR/dT exhibits a special pressure dependence. At present, we can unveil the physical mechanism of how the pressure affects the R and dR/dT of Al. Firstly, pressure enlarges the ΔE_{ul}, thereby increasing the energy threshold for interband transitions. Then, the lifted energy threshold alters the optical absorption rates at the probe beam photon energy. Finally, the change in probability of interband transitions makes the R and dR/dT to exhibit pressure-dependent behaviors.

Conclusions

In conclusion, we have unveiled the correlation between pressure and optical properties of Al by combining TDTR experiments and dielectric function theory. The reflectivity R of Al nano-films can be affected by the shear strains of Al/substrate interfaces, which altered the Fermi level. On the contrary,
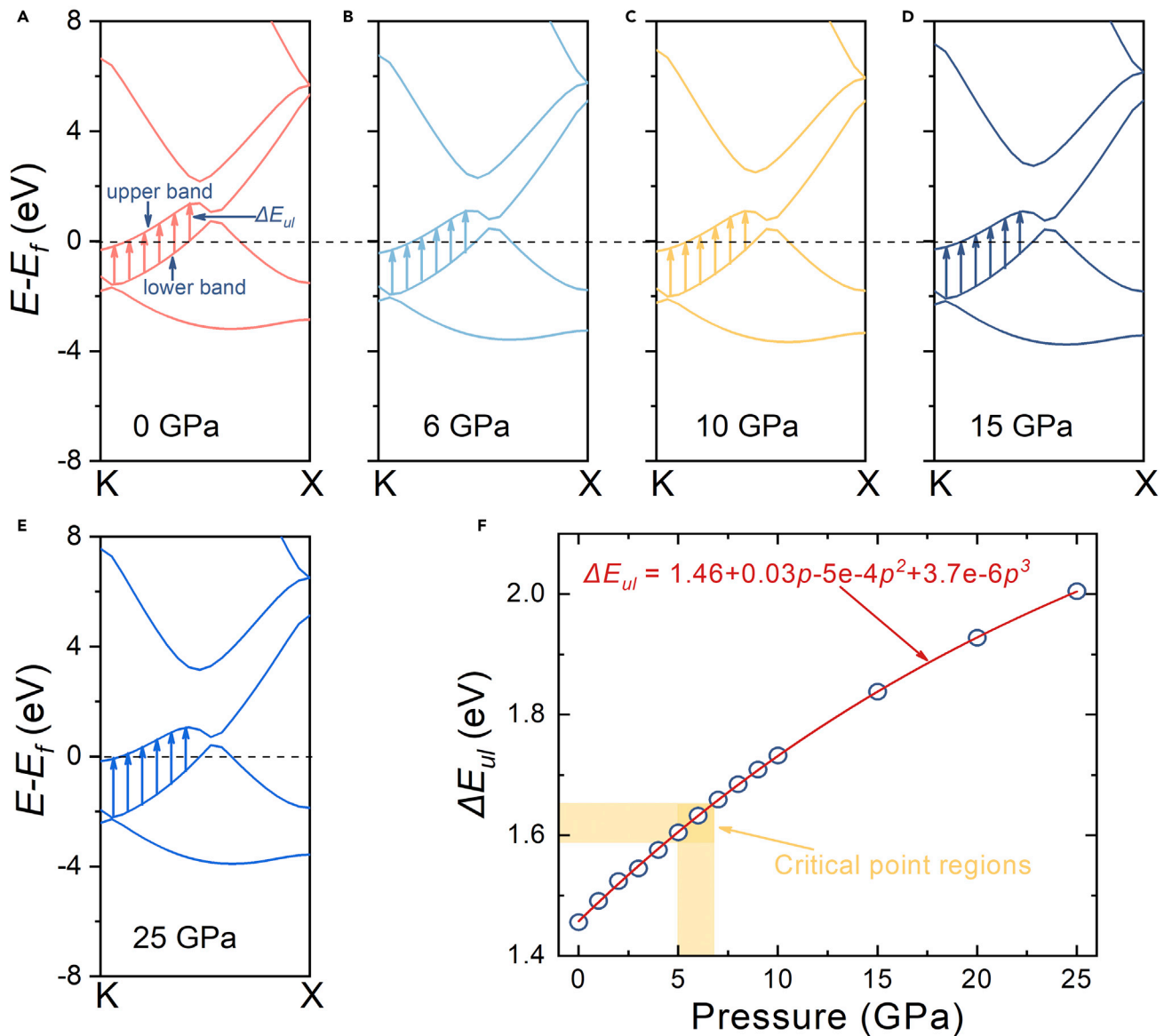
Figure 4. First-principles calculations for Al band structure under high-pressure

(A–E) Band structure of Al between **K** and **X** points at the pressure of 0, 6, 10, 15, and 25 GPa, respectively. E_f denotes the Fermi level (dash line), ΔE_{ul} is the energy difference of the upper and lower bands, and the arrows depict the region where the strongest interband transitions take place.

(F) ΔE_{ul} as a function of pressure. We fit ΔE_{ul} and pressure by a 3rd polynomial fitting for guiding the eyes. In addition, the critical point regions, where dR/dT is tuned from positive to negative, are labeled.

the shear strain effect on the thermoreflectance dR/dT is not significantly noticed. The dR/dT as well as reflectivity temperature coefficients of electrons and phonons in Al are changed from positive to negative with the increasing pressure, and the zero-crossing appears at 5–7 GPa. This phenomenon can be explained thoroughly: (i) pressure enlarges the energy difference of the parallel bands between **K** and **X** points in the Brillouin zone from 1.45 to 2 eV, thereby increasing the threshold for electronic transitions. (ii) The lifted threshold changes the optical absorption rates of Al as well as the density of states of the electrons that involve interband transitions; as a result, R and dR/dT exhibit such pressure-dependent behaviors. (iii) The light is absorbed mightily at 5–7 GPa for the resonance effect, so that the dR/dT is changed from positive to negative. Our results provide both a deep insight on pressure-induced electronic transitions and photon-electron interactions in metals and an important guidance for TDTR to accurately characterize thermal transport properties under high pressure.
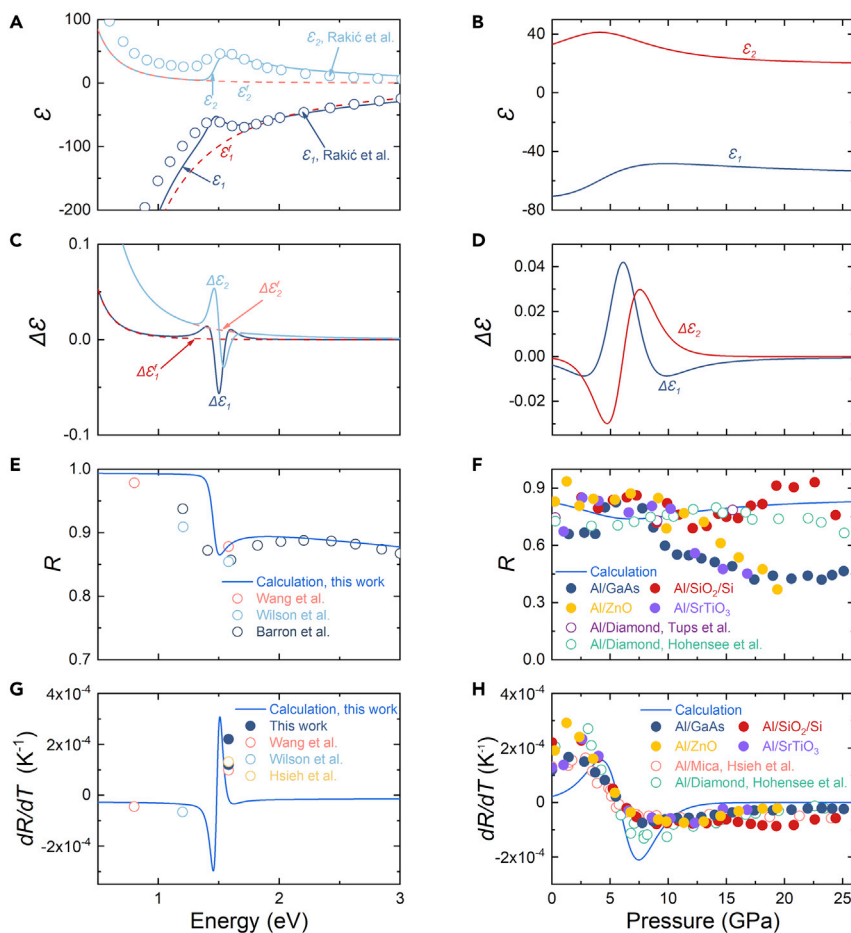
Figure 5. Theoretical results of dielectric function, *R*, and *dR/dT* as functions of photon energy and pressure

(A, C, E, and G) The dielectric function, *R*, and *dR/dT* of Al as functions of photon energy. ϵ is the dielectric function and $\Delta\epsilon$ the change in the dielectric function. Subscripts 1 and 2 denote real and imaginary parts of complex dielectric function. Superscript *f* represents free electrons involving intraband transitions.

(B, D, F, and H) The ϵ, $\Delta\epsilon$, *R*, and *dR/dT* of Al as functions of pressure. Solid lines denote our calculation results. Filled and hollow circles represent the experimental results from this work and literature, respectively.

Limitations of the study

At present, it is difficult to accurately characterize the band structure of materials under high pressure. Pressure-dependent optical properties of other metals need to be further investigated in experiments. Even though the theoretical model built in this work is able to give an accurate quantitative description to the optical properties of Al, a more perfect model, in which indirect electron transitions are taken into consideration, is needed in the future for the better description of other metals and semiconductors. In addition, the thickness of metal films (less than 50 nm) is also a key factor to affect optical constants, such as refractive index and dielectric constants. Investigations on thickness-dependent optical constants under high-pressure conditions is an important and interesting research field, which need be further studied in the future.

STAR★METHODS

Detailed methods are provided in the online version of this paper and include the following:

- KEY RESOURCES TABLE
- RESOURCE AVAILABILITY
  - Lead contact
  - Materials availability

SUPPLEMENTAL INFORMATION

Supplemental information can be found online at https://doi.org/10.1016/j.isci.2021.102990.

AUTHOR CONTRIBUTIONS

Conceptualization, Z.Z., J.Z., and D.T.; Methodology, Z.Z., Z.C., and X.Z.; Investigation, Z.Z., X.F., J.Z., and X.W.; Writing – Original Draft, Z.Z.; Writing – Review & Editing, Z.Z., J.Z., and D.T.; Funding Acquisition, J.Z. and D.T.; Supervision, J.Z. and D.T.

DECLARATION OF INTEREST

The authors declare no competing interests.

REFERENCES

Barron, L.W., Neidrich, J., and Kurinec, S.K. (2007). Optical, electrical, and structural properties of sputtered aluminum alloy thin films with copper, titanium and chromium additions. Thin Solid Films 515, 3363–3372.

Braun, J.L., Szwejkowski, C.J., Giri, A., and Hopkins, P.E. (2018). On the steady-state temperature rise during laser heating of multilayer thin films in optical pump–probe techniques. J. Heat Transfer 140, 052801–052810.

Cahill, D.G. (2004). Analysis of heat flow in layered structures for time-domain thermoreflectance. Rev. Sci. Instrum. 75, 5119–5122.

Chen, J.-Y., Zhu, J., Zhang, D., Lattery, D.M., Li, M., Wang, J.-P., and Wang, X. (2016). Time-resolved magneto-optical kerr effect of magnetic thin films for ultrafast thermal characterization. J. Phys. Chem. Lett. 7, 2328–2332.

Colavita, E., Franciosi, A., Lynch, D.W., Paolucci, G., and Rosei, R. (1983a). Thermoreflectance investigation of the antiferromagnetic and paramagnetic phases of Cr. Phys. Rev. B 27, 1653–1663.

Colavita, E., Franciosi, A., Mariani, C., and Rosei, R. (1983b). Thermoreflectance test of W, Mo, and paramagnetic Cr band structures. Phys. Rev. B 27, 4684–4693.

Dandrea, R.G., and Ashcroft, N.W. (1985). High pressure as a probe of electron structure: Aluminum. Phys. Rev. B 32, 6936–6938.

Eesley, G.L. (1983). Observation of nonequilibrium electron heating in copper. Phys. Rev. Lett. 51, 2140–2143.

Ehrenreich, H., Philipp, H.R., and Segall, B. (1963). Optical properties of aluminum. Phys. Rev. 132, 1918–1928.

Favaloro, T., Bahk, J.-H., and Shakouri, A. (2015). Characterization of the temperature dependence of the thermoreflectance coefficient for conductive thin films. Rev. Sci. Instrum. 86, 024903.

Hanus, J., Feinleib, J., and Scouler, W.J. (1967). Low-energy interband transitions and band structure in nickel. Phys. Rev. Lett. 19, 16–20.

Hohensee, G.T., Hsieh, W.-P., Losego, M.D., and Cahill, D.G. (2012). Interpreting picosecond acoustics in the case of low interface stiffness. Rev. Sci. Instrum. 83, 114902.

Hohensee, G.T., Fellinger, M.R., Trinkle, D.R., and Cahill, D.G. (2015a). Thermal transport across high-pressure semiconductor-metal transition in Si and $Si_{0.991}Ge_{0.009}$. Phys. Rev. B 91, 205104.

Hohensee, G.T., Wilson, R.B., and Cahill, D.G. (2015b). Thermal conductance of metal–diamond interfaces at high pressure. Nat. Commun. 6, 6578.

Hopkins, P.E. (2009). Effects of electron-boundary scattering on changes in thermoreflectance in thin metal films undergoing intraband excitations. J. Appl. Phys. 105, 093517.

Hopkins, P.E. (2010a). Influence of electron-boundary scattering on thermoreflectance calculations after intra- and interband transitions induced by short-pulsed laser absorption. Phys. Rev. B 81, 035413.

Hopkins, P.E. (2010b). Thermoreflectance dependence on Fermi surface electron number density perturbations. Appl. Phys. Lett. 96, 041901.

Hostetler, J.L. (2001). Investigation of Femtosecond Transient Thermoreflectance Technique Applied to Characterization of Microscale Heat Transfer Properties in Thin Films (University of Virginia).

Hsieh, W.-P., and Cahill, D.G. (2011). Ta and Au(Pd) alloy metal film transducers for time-domain thermoreflectance at high pressures. J. Appl. Phys. 109, 113520.

Hsieh, W.-P., Lyons, A.S., Pop, E., Keblinski, P., and Cahill, D.G. (2011). Pressure tuning of the thermal conductance of weak interfaces. Phys. Rev. B 84, 184107.

Hu, E.-T., Cai, Q.-Y., Zhang, R.-J., Wei, Y.-F., Zhou, W.-C., Wang, S.-Y., Zheng, Y.-X., Wei, W., and Chen, L.-Y. (2016). Effective method to study the thickness-dependent dielectric functions of nanometal thin film. Opt. Lett. *41*, 4907–4910.

Hummel, R.E. (2011). Electronic Properties of Materials (Springer Science & Business Media).

Jaffe, A., Lin, Y., Beavers, C.M., Voss, J., Mao, W.L., and Karunadasa, H.I. (2016). High-pressure single-crystal structures of 3D lead-halide hybrid perovskites and pressure effects on their electronic and optical properties. ACS Cent. Sci *2*, 201–209.

Jayaraman, A. (1986). Ultrahigh pressures. Rev. Sci. Instrum. *57*, 1013–1031.

Kaveh, M., and Wiser, N. (1984). Electron-electron scattering in conducting materials. Adv. Phys. *33*, 257–372.

Klotz, S., Chervin, J.C., Munsch, P., and Le Marchand, G. (2009). Hydrostatic limits of 11 pressure transmitting media. J. Phys. D: Appl. Phys. *42*, 075413.

Kresse, G., and Furthmüller, J. (1996). Efficient iterative schemes for ab initio total-energy calculations using a plane-wave basis set. Phys. Rev. B *54*, 11169–11186.

Liu, S., Li, X., Wang, D., Wu, M., Yin, G., and Li, M. (2020). Mechanical and acoustic emission characteristics of coal at temperature impact. Nat. Resour. Res. *29*, 1755–1772.

Mao, H.-K., Chen, X.-J., Ding, Y., Li, B., and Wang, L. (2018). Solids, liquids, and gases under high pressure. Rev. Mod. Phys. *90*, 015007.

Perdew, J.P., Burke, K., and Ernzerhof, M. (1996). Generalized gradient approximation made simple. Phys. Rev. Lett. *77*, 3865–3868.

Radue, E.L., Tomko, J.A., Giri, A., Braun, J.L., Zhou, X., Prezhdo, O.V., Runnerstrom, E.L., Maria, J.-P., and Hopkins, P.E. (2018). Hot electron thermoreflectance coefficient of gold during electron–phonon nonequilibrium. ACS Photon. *5*, 4880–4887.

Rakić, A.D., Djurišić, A.B., Elazar, J.M., and Majewski, M.L.J.A.O. (1998). Optical properties of metallic films for vertical-cavity optoelectronic devices. Appl. Opt. *37*, 5271–5283.

Rosei, R. (1974). Temperature modulation of the optical transitions involving the Fermi surface in Ag: Theory. Phys. Rev. B *10*, 474–483.

Rosei, R., Culp, C.H., and Weaver, J.H. (1974). Temperature modulation of the optical transitions involving the Fermi surface in Ag: Experimental. Phys. Rev. B *10*, 484–489.

Rosei, R., and Lynch, D.W. (1972). Thermomodulation spectra of Al, Au, and Cu. Phys. Rev. B *5*, 3883–3894.

Smith, A.N., and Norris, P.M. (2001). Influence of intraband transitions on the electron thermoreflectance response of metals. Appl. Phys. Lett. *78*, 1240–1242.

Smith, N.V. (1971). Photoelectron energy spectra and the band structures of the noble metals. Phys. Rev. B *3*, 1862–1878.

Tups, H., and Syassen, K. (1984). Effect of pressure on the optical absorption in aluminium. J. Phys. F: Metal Phys. *14*, 2753–2767.

Wang, Y., Park, J.Y., Koh, Y.K., and Cahill, D.G. (2010). Thermoreflectance of metal transducers for time-domain thermoreflectance. J. Appl. Phys. *108*, 043507.

Wilson, R.B., Apgar, B.A., Martin, L.W., and Cahill, D.G. (2012). Thermoreflectance of metal transducers for optical pump-probe studies of thermal properties. Opt. Express *20*, 28829–28838.

Xiao, G., Cao, Y., Qi, G., Wang, L., Liu, C., Ma, Z., Yang, X., Sui, Y., Zheng, W., and Zou, B. (2017). Pressure effects on structure and optical properties in cesium lead bromide perovskite nanocrystals. J. Am. Chem. Soc. *139*, 10087–10094.

Zhao, Y.S., Wan, Z.J., Feng, Z.J., Xu, Z.H., and Liang, W.G. (2017). Evolution of mechanical properties of granite at high temperature and high pressure. Geomech. Geophys. Geo-energy Geo-resour. *3*, 199–210.

Zhang, L., Li, W., Zhang, L., Zhong, Y., Guo, X., Li, L., Wang, E.N., and Guo, L. (2020). Framework for analyzing the thermoreflectance spectra of metal thermal transducers with spectrally tunable time-domain thermoreflectance. J. Appl. Phys. *128*, 055107.

Zheng, W., Nemilentsau, A., Lattery, D., Wang, P., Low, T., Zhu, J., and Wang, X. (2018). Direct investigation of the birefringent optical properties of black phosphorus with picosecond interferometry. Adv. Opt. Mater. *6*, 1700831.

Zhu, J., Wu, X., Lattery, D.M., Zheng, W., and Wang, X. (2017). The ultrafast laser pump-probe technique for thermal characterization of materials with micro/nanostructures. Nanoscale Microscale Thermophys. Eng. *21*, 177–198.

STAR★METHODS

KEY RESOURCES TABLE

REAGENT or RESOURCE	SOURCE	IDENTIFIER
Chemicals, peptides, and recombinant proteins		
Gallium arsenide	Hefei kejing materials technology Co., China	CAS: 1303-00-0
Silica	Hefei kejing materials technology Co., China	CAS: 112945-52-5
Strontium titanate	Hefei kejing materials technology Co., China	CAS: 12060-59-2
Zinc oxide	Hefei kejing materials technology Co., China	CAS: 1314-13-2
Silicone oil	Aladdin Industrial Co., China	CAS: 63148-62-9
Software and algorithms		
Origin 2018	Originlab	https://www.originlab.com/
Vienna Ab-initio Simulation Package (VASP)	National Supercomputing Center in Shenzhen	http://www.nsccsz.cn/
MATLAB 2018a	Mathworks	https://www.mathworks.com/

RESOURCE AVAILABILITY

Lead contact

Further information and requests for resources and reagents should be directed to and will be fulfilled by the Lead Contact, Jie Zhu (zhujie@dlut.edu.cn).

Materials availability

This study did not generate new unique reagents.

Data and code availability

- Data reported in this paper will be shared by the lead contact upon request.

- This paper does not report original codes. Computational algorithms are written in the STAR Methods.

- Any additional information required to reanalyze the data reported in this paper is available from the lead contact upon request.

METHOD DETAILS

Sample preparations

We used commercial <100> GaAs [N-type (phosphorus), 10^{-3} $\Omega \times$cm resistivity], thermally oxidized Si wafers, zinc oxide (ZnO <0001>), and strontium titanate (SrTiO$_3$ <100>) as the substrate materials. The thickness of the SiO$_2$ layer was measured by an ellipsometer as 327 $\pm$ 3 nm. Before further processing, the thickness of GaAs, SiO$_2$/Si, ZnO, and SrTiO$_3$ were polished to $\approx$20 μm, so that they were able to be loaded into the DAC smoothly. To remove surface impurities, we treated these four kinds of substrates in the hydrogen atmosphere in a tube furnace at 800 K for 30 min. Then the Al film was deposited on these substrates by a dc magnetron sputtering, and the thickness of Al was about 96 nm measured by picosecond acoustics (Hohensee et al., 2012) at ambient condition. The Al film is optically thick and should reflect the same optical constant as bulk materials (Hu et al., 2016). Therefore, we did not suppose any thickness dependence or size effect here. After sputtering, the samples were fractured to squares of size 60 × 60 μm by a tungsten needle, and then loaded into a DAC together with some ruby spheres (diameter $\approx$10 μm) and silicone-oil. The ruby fluorescence was used as a pressure sensor to calibrate pressure and the silicone-oil acted as the pressure transmission medium, which ensured the samples in a quasi-hydrostatic environment (Mao et al., 2018). The electronic conductivity of the Al film was determined by the four-point probe technique on another reference piece due to the small sizes and fragility of the samples in the DAC. Then the Al-film thermal conductivity was calculated as 120 Wm^{-1}K^{-1} through the Wiedemann-Franz law.

In addition, we verify the quasi-hydrostatic environment. Several ruby spheres were placed at different locations in the DAC and we measured the fluorescence spectra of each ball to determine the pressure gradient. The statistical precision on the position is ± 0.1 cm^{-1} corresponding to ± 0.015 GPa. An extremely sensitive and reliable criterion for pressure gradients is the standard deviation σ of the P_i indicated by ruby spheres (Klotz et al., 2009) as $\sigma = \sqrt{1/N\sum_{i=1}^{N}(Pi - \overline{P})^2}$, where N is the number of ruby spheres and $\overline{P}$ the average pressure. The percentage of pressure gradient relative to $\overline{P}$ was shown in Figure S1, and obviously, the pressure gradient is within 5%, evidencing the quasi-hydrostatic environment.

Time domain thermoreflectance tests

In our experiment, TDTR integrated with DAC were employed to measure the R and dR/dT of Al nano-films under high pressure. A schematic of the TDTR optical path and the internal structure of DAC in use at the Dalian University of Technology are shown in Figure 1.

In our TDTR system (Zhu et al., 2017), the output of a mode-locked Ti:sapphire laser, which is of 785 nm wavelength, 280 fs pulse width and at a repetition rate of 80 MHz, is split into a pump beam and a probe beam through a polarizing beam splitter. The pump beam is modulated at the frequency of 9.8 MHz and creates a temperature rise at the surface of the metal film. The probe beam, which is mechanically chopped at audio frequency to remove background noise created by coherent pick-up and diffusely, subsequently monitors the small changes in optical reflectivity due to the temperature evolution of the metal film surface. A mechanical delay stage advances the arrival time of the pump beam relative to the probe beam. The pump and probe beams are geometrically collinear and focus on the sample producing a beam spot size (12 μm of 1/e^2 radii) by 5× objective lens. The reflected probe beam is collected by a fast-response photodiode detector. Before entering a lock-in amplifier, the voltage signals pass through a resonant filter and a preamplifier. The root-mean-square (rms) voltage V_m is measured by the lock-in amplifier, and the real and imaginary parts of the V_m are given by an in-phase (V_{in}) signal and an out-of-phase (V_{out}) signal. Meanwhile, a dc voltage (V_{dc}) generated by the photodiode is collected. To guarantee the validity of V_m and V_{dc} signals, we fix the incident power of the pump and probe beams at 20 and 10 mW, respectively. It is worth mentioning that V_m and V_{dc} represent the change in reflectivity caused by temperature rise and the static reflectivity, respectively, and enable us to derive the dR/dT and R of the metal transducer.

Here, we determined the R of the Al nano-films in two steps. First, on the basis of the Fresnel equation for the normal incidence, we calculated the R of the silicone-oil/Al interface. Then, V_{dc} signals represented the R, and we compared the V_{dc} signals of different pressure to that of ambient pressure so that the R of different pressure can be estimated. Therefore, we calculated R at different pressure from the following relationship:

$$R = \frac{V_{dc,p}}{V_{dc,0}}R_0 \qquad \text{(Equation 1)}$$

from which we can get $R_0 = 0.83$, the reflectivity of the silicone-oil/Al interface at ambient pressure, $V_{dc,0}$ represents the rms dc signals at ambient pressure, and $V_{dc,p}$ denotes the dc signals at different pressure (p). We determined dR/dT based on the equation derived by Cahill (Cahill, 2004) and Wang et al. (Wang et al., 2010), and dR/dT was quantified by

$$\frac{dR}{dT} = \frac{\sqrt{2}}{Q}\frac{V_m(t)}{V_{dc}}\frac{R}{\Delta T(t)}, \qquad \text{(Equation 2)}$$

where $Q \approx 12$ is the quality factor of the resonant circuit for our TDTR system at the modulation frequency $f = 9.8$ MHz. $V_m(t)$ is the voltage measured by the RF lock-in amplifier at a delay time $t = 100$ ps, which ensures electrons and phonons in thermal equilibrium. $\Delta T(t = 100\text{ ps}) \approx 0.8$ K is the temperature rise at the delay time calculated through the bidirectional heat transfer model outlined by Braun et al. (Braun et al., 2018).

Theoretical model details

In the interaction between photons and electrons, intraband transitions represent that free electrons are excited into a higher energy level within the same band and mainly are promoted in the near infrared regime. In contrast, interband transitions represent that bound electrons are excited into a higher energy band which is unoccupied. Note that indirect interband transitions are disregarded for the interpretation of

metal spectrum, because they are generally weaker than direct transitions by two or three orders of magnitude.

In this section, we briefly derived the theoretical expression of the R and dR/dT of Al and developed the quantum mechanics model that investigated the pressure effect on the R and dR/dT of Al. The expression of R needs to be derived first. On the basis of the Fresnel equation, we carried out the relationship of the R and dielectric constant as (Rakić et al., 1998):

$$R = \frac{\sqrt{\epsilon_1^2 + \epsilon_2^2} + n_0^2 - n_0 \sqrt{2\left(\sqrt{\epsilon_1^2 + \epsilon_2^2} + \epsilon_1\right)}}{\sqrt{\epsilon_1^2 + \epsilon_2^2} + n_0^2 + n_0 \sqrt{2\left(\sqrt{\epsilon_1^2 + \epsilon_2^2} + \epsilon_1\right)}}$$ (Equation 3)

where ϵ_1 and ϵ_2 are the real and imaginary components of the dielectric function, respectively, and $n_0 = 1.4$ the refractive index of the Silicone-oil. With the classical Drude model and Lorentz model used, the complex dielectric function was given by (Hostetler, 2001; Hummel, 2011)

$$\epsilon = \epsilon_1 - i\epsilon_2 = \epsilon^f + \epsilon^b = \left(\epsilon_1^f + \epsilon_1^b\right) - i\left(\epsilon_2^f + \epsilon_2^b\right),$$ (Equation 4)

$$\epsilon^f = \epsilon_1^f - i\epsilon_2^f = \left(1 - \frac{\omega_p^2}{\omega^2 - \omega_c^2}\right) + i\left(\frac{\omega_c}{\omega}\frac{\omega_p^2}{\omega^2 - \omega_c^2}\right),$$ (Equation 5)

$$\epsilon^b = \epsilon_1^b - i\epsilon_2^b = \sum_i \frac{f_i\omega_p^2\left(\omega_{ul}^2 - \omega^2\right)}{\left(\omega_{ul}^2 - \omega^2\right)^2 + \omega^2\omega_c^2} - i\left(\sum_i \frac{f_i\omega_p^2\omega\omega_c}{\left(\omega_{ul}^2 - \omega^2\right)^2 + \omega^2\omega_c^2}\right)$$ (Equation 6)

where ϵ is complex dielectric function. The superscripts of f and b denote free and bound electrons, respectively. ω is the frequency of the probe beam, ω_p the plasma frequency, and ω_c the collision frequency. The f_i represents scattering strength of a number of i oscillators, and the resonance frequency ω_{ul}, a function of pressure, is associated with the transition between the lower (by the subscript of l) and upper (by the subscript of u) bands. We expect that the change of ω_p as functions of temperature and pressure is negligible for it small enough (Radue et al., 2018). The ω_c is linearly dependent on temperature when electrons and phonons are in thermal equilibrium and is expressed as (Kaveh and Wiser, 1984; Zhang et al., 2020)

$$\omega_c = \gamma T,$$ (Equation 7)

where γ is 2.38×10^{11} radK^{-1}s^{-1} for Al (Kaveh and Wiser, 1984) and T the temperature. Note that the electron-electron collision frequency is too small to be considered (Radue et al., 2018), and the electron-phonon collision frequency is dominated by temperature merely. The resonance frequency ω_{ul} described in Equation 6 is related to interband transitions and is pressure-dependent. In the calculation on pressure-dependent R, we, therefore, set the ω_c as a constant (7.14×10^{13} rad/s) (Kaveh and Wiser, 1984). The relationship between R and pressure can be concluded as: 1) R is a function of the dielectric function (Equation 3); 2) Dielectric function includes intraband transitions (Equation 4) and interband transitions (Equation 6); 3) Intraband transitions are pressure-independent and ω_{ul} invoving interband transitions is pressure-dependent. Hence, on the basis of Equations (3)–(7), we can obtain the relationship between R and pressure.

To clarify the relationship of dR/dT with pressure, photon energy, and temperature due to interband transitions, we propose a quantum mechanical approach on the basis of the optical transition theory (Rosei, 1974), and it is utilized and reiterated below:

$$\epsilon_2^b(p, \hbar\omega, T) = \frac{8\pi^2 e^2 \hbar^4}{3m^2} \frac{|P|^2}{(\hbar\omega)^2} \mathfrak{J}'_{ul}(p, \hbar\omega, T)$$ (Equation 8)

$$\mathfrak{J}'_{ul}(p, \hbar\omega, T) = \frac{\sqrt{m^3}}{4\pi^2\hbar^3}\left(1 - F(\hbar\omega - \Delta E_{ul}(p), T)\right)$$
$$= \frac{\sqrt{m^3}}{4\pi^2\hbar^3}\left[1 - \frac{1}{e^{\frac{(\hbar\omega - \Delta E_{ul}(p))}{k_B T}} + 1}\right],$$ (Equation 9)

where P is the momentum-matrix-element which is assumed constant for each transition and m the effective mass of the electron (Smith, 1971). $\mathfrak{J}'_{ul}(p, \hbar\omega, T)$ is weighted joint-density-of states for an interband transition terminating at the Fermi energy. $\Delta E_{ul} = E_u - E_l$ is the energy difference between the upper and lower bands and is a function of pressure, $\hbar\omega$ the photon energy of the probe beam, and k_B the Boltzmann

constant. On the basis of Equation (9), we found that the imaginary part of the dielectric function involving interband transitions was directly proportional to the Fermi distribution of unoccupied states and inversely proportional to the photon energy of the probe beam. With adopting the Kramers-Kronig relations (Ehrenreich et al., 1963), we obtained the real part of dielectric function due to interband transitions,

$$\epsilon_1^b(\hbar\omega, T, p) = \frac{2}{\pi} \int_0^\infty \frac{\hbar\omega' \epsilon_2^b(p, \hbar\omega', T)}{(\hbar\omega')^2 - (\hbar\omega)^2} d\hbar\omega', \quad \text{(Equation 10)}$$

where ω' is a virtual integral variable and the Equation (10) can be numerically integrated once ϵ_2^b is determined. Temperature induced the change of the R can be expressed linearly as

$$\frac{dR}{dT} \approx \frac{\Delta R}{\Delta T} = \left(\frac{\partial R}{\partial \epsilon_1}\right) \frac{\Delta \epsilon_1}{\Delta T} + \left(\frac{\partial R}{\partial \epsilon_2}\right) \frac{\Delta \epsilon_2}{\Delta T}, \quad \text{(Equation 11)}$$

and when ΔT is small enough, the change of real and imaginary parts of the complex dielectric constant is given by

$$\Delta\epsilon_1 = \Delta\epsilon_1^f + \Delta\epsilon_1^b,$$
$$\Delta\epsilon_2 = \Delta\epsilon_2^f + \Delta\epsilon_2^b. \quad \text{(Equation 12)}$$

Therefore, the change of the imaginary part of the dielectric constant involving interband transitions can be expressed as

$$\frac{\Delta\epsilon_2^b(p, \hbar\omega, T)}{\Delta T} = \frac{8\pi^2 e^2 \hbar^4}{3m^2} \frac{|P|^2}{(\hbar\omega)^2} \frac{\partial \Im'_{lu}(p, \hbar\omega, T)}{\partial T}, \quad \text{(Equation 13)}$$

and the change of the real part of the dielectric constant was calculated by the Kramers-Kronig relations. According to Equations 8–13 and the Kramers-Kronig relations, we can obtain the complex expression of dR/dT involving $\Delta E_{ul}(p)$, $\hbar\omega$, and T. In this work, our experiment is performed at room temperature and fixed photon energy (1.58 eV), therefore, p is the only key factor to affect ΔE_{ul}, which makes dR/dT exhibit a pressure dependent behavior.

In order to make the relationship between dR/dT and pressure clearer, we conclude this relationship as: the weighted JDOS $\Im'_{ul}$ is directly related to the band difference ΔE_{ul}, which is a function of pressure (Equation 9). Then we can obtain the pressure-dependent ϵ_2^b (Equation 8) as well as $\Delta\epsilon_2^b$ (Equation 13), and with the Kramers-Kronig relations using, pressure-dependent ϵ_1^b and $\Delta\epsilon_1^b$ are calculated. Hence, on the basis of the Equation 11, we can obtain the relationship between dR/dT and the externally applied pressure.

First-principles calculations

To determine ΔE_{ul}, which makes the R and dR/dT of Al exhibit pressure dependent behaviors, we calculated the band structure of Al from ambient pressure to 25 GPa using *first-principles* calculations. We first performed the structural optimization of Al, within the framework of density functional theory using Perdew–Burke–Ernzerhof (PBE) exchange correlation functional (Perdew et al., 1996) as implemented in Vienna *ab initio* simulation package (VASP) (Kresse and Furthmüller, 1996). For the plane wave expansion in reciprocal space, we set 400 eV as the kinetic energy cutoff value, and the energy convergence threshold for the total energy difference between two successive self-consistency steps is 10^{-8} eV. The k-mesh employed in the first Brillouin zone was 22 × 22×22, generated by a Γ-centered method. The geometrical structure was fully relaxed until all atomic forces less than 10^{-5} eVÅ^{-1}. While an external pressure was applied to the unit cell, the lattice constants reduced isotropically and the positions of Al atoms in it shifted in order to guarantee the electronic potential of the new structure to balance the external pressure on the boundary. We then calculated the pressure-dependent band structure using the above optimized unit cell, and the Brillouin zone path was set as Γ-X-W-L-Γ-K-X.

QUANTIFICATION AND STATISTICAL ANALYSIS

Each experimental value of R and dR/dT of this work shown in Figures 2, 3 and 5 of the main manuscript corresponds to the average value obtained from multiple measurements at a given pressure and the error are the root-mean-square error.